Georgia Institute of Technology
Atlanta, Georgia 30332

ACTIVELY CONTROLLED SHAFT SEALS FOR AEROSPACE APPLICATIONS

Semiannual Status Report, July - December, 1992

NASA Research Grant NAG 3-974

Principal Investigator Richard F. Salant
College of Engineering
School of Mechanical Engineering

NASA Technical Officer: M.P. Proctor
NASA Lewis Research Center, MS SPT D-2
Space Vehicle Propulsion Branch

E25-666

SUMMARY

The major objective of year 4 of this project (1992) was to determine experimentally the steady state behavior and operating characteristics of a controllable mechanical seal. That objective was achieved. The results and background to the work are described below.

NOMENCLATURE

F_{close} = closing force

F_{open} = opening force

h = film thickness

k = film stiffness

m = leakage rate (in terms of mass flow rate)

P = pressure

P^* = dimensionless pressure, $[(P^2 - P_i^2) / (P_o^2 - P_i^2)]^{1/2}$

Q = viscous heat generation rate

r = radial coordinate

r^* = dimensionless radial coordinate, r / r_i

R = gas constant

T = temperature

V = volume

v = voltage

$\alpha^* =$ radius ratio, $r_i / (r_o - r_i)$

$\beta =$ slope of seal face

$\delta =$ coning, $h_o - h_i$

$\delta^* =$ dimensionless coning, δ / h_i

$\mu =$ viscosity

$\omega =$ rotational speed

Subscripts

i= inner radius

o= outer radius

INTRODUCTION

Most modern mechanical seals are designed to operate with full film lubrication between the mating faces, under steady state conditions at the design point. The presence of a thin lubricating film, with a thickness on the order of a few microns, minimizes wear and the occurrence of mechanical and thermal damage to the faces. However, under transient and off-design conditions the lubricating film frequently breaks down, resulting in mechanical contact between the faces. To prevent face contact, a new class of "controllable" mechanical seals has been under study and development by several researchers (1-4). In such seals the film thickness is adjustable, so that it can be increased when face contact is imminent and decreased when leakage is excessive.

The previous work on controllable mechanical seals, mentioned above, has been directed toward industrial applications. The present work is directed toward demonstrating the feasibility of such seals for aerospace applications in which size and weight constraints are extremely severe. As a demonstration application, the purge gas seals in a liquid oxygen turbopump has been chosen. Figure 1 shows a typical helium purge gas seal assembly, with floating ring seals, that is normally used in turbopumps. Pressurized helium enters at the midpoint, leaks through the seal clearances along the shaft, and exits through the drains. The helium therefore prevents the hot gases on the turbine side of the turbopump from contacting the oxygen on the pump side. The disadvantage of this arrangement is: the floating ring clearances must be large, on the order of twenty microns, resulting in a high leakage rate.

Figure 2 shows a conventional double mechanical seal arrangement that would be a suitable low-leakage replacement for the floating ring seals. The nonrotating carbon faces (in holders) float, and are free to move in the axial direction. The rotating face is fixed axially. Such seals are normally designed to run with a one to five micron lubricating film of fluid separating the faces. However, if there is a transient or if environmental conditions change, the film can break down, and face contact occur, resulting in damage to the faces. The purpose of the electronically controlled mechanical seal is to prevent such face contact by controlling the thickness of the lubricating film.

It should be noted that the size and operating conditions of a liquid oxygen turbopump impose severe constraints on the design of a controllable mechanical seal. The dimensions of the seal

envelope are 3.81 cm in the axial direction and 1.27 cm from the outside radius of the shaft to the outside radius of the envelope. These dimensions are considerably smaller than those of previous controlled seals. The high and low pressure sides of the seal are at 1.48×10^6 Pa (200 psig) and 1.01×10^5 Pa (0 psig), respectively. The shaft of the turbopump rotates at a speed of 7,330 rad/sec (70,000 rpm).

PRINCIPAL OF OPERATION AND SEAL CONFIGURATION

In a conventional mechanical seal the film thickness is determined by the location of the floating seal face, which is determined by the forces acting on it. The sealed pressure acting on the backside of the face and the spring produce a closing force, which tends to close the gap between the faces. Opposing the closing force is an opening force, which is produced by the pressure distribution in the lubricating film. One could therefore control the film thickness by controlling either the closing force (4) or the opening force (1). In the present work, it is the opening force that is controlled.

To regulate the opening force, it is necessary to control the pressure distribution in the lubricating film. That pressure distribution is strongly influenced by the geometry of the surfaces of the seal faces. In a conventional seal, the faces are not parallel but are coned due to mechanical and thermal deformation. This coning is very small, on the order of microns. In a hydrostatic seal, the larger the coning, normalized with respect to the average film thickness, the more convex the pressure distribution and the larger the opening force (1). However, under

steady state conditions the opening force must equal the closing force. Therefore the average steady state film thickness will be proportional to the coning: the larger the coning, the larger the film thickness. In the electronically controlled seal, the film thickness is controlled by controlling the coning.

Figure 3 shows such an electronically controlled seal. It is similar to the conventional seal of Fig. 2, except the carbon face is replaced with a deformable face assembly. That assembly consists of a thin carbon face bonded to a piezoelectric element. When a voltage is applied to the piezoelectric element, the piezoelectric crystal deforms in the shear mode and skews, thereby producing positive coning of the carbon face. The larger the applied voltage, the larger the coning and the thicker the lubricating film. Therefore, by adjusting the voltage, one can adjust the film thickness.

To determine how much voltage should be applied to the piezoelectric element for optimum operation at any given instant of time, information on the conditions in the fluid film and the sealed cavity is required. Those conditions are monitored by a thermocouple imbedded in the carbon face to measure face temperature, and another thermocouple in the sealed cavity. The outputs of these thermocouples could serve as inputs to an electronic control system that generates a commanded actuator voltage. Alternatively, the output of a leakage rate monitor could be used as input to the control system.

MATHEMATICAL MODEL AND ANALYTICAL RESULTS

Since the proposed electronically controlled seal must be very compact and meet extreme performance specifications, a computerized mathematical model of the seal was constructed to optimize the design. The mathematical model consists of four major elements: a force balance, fluid mechanics model, heat transfer and structural model, and an overall computational procedure. The performance characteristics of primary interest are the film thickness and leakage rate for a range of voltage applied to the piezoelectric element. The model assumes steady state operation of the seal.

The first step in computing the film thickness is to perform a force balance on the floating component ($F_{open} = F_{close}$). Computation of the closing force is straightforward. However, to determine the opening force, the pressure distribution within the fluid film must be computed from the relevant fluid mechanics equations.

The pressure distribution is governed by the Navier-Stokes equations. An analytical expression can be obtained from these equations when the following simplifying assumptions are made (5): steady state, axisymmetric fluid film, isothermal fluid film, ideal gas behavior, laminar flow, no centrifugal effects, no velocity gradients in the radial direction, and no squeeze film effects. Using these assumptions,

$$(P^*)^2=[lnr^*-\ln(1+\delta^*\alpha^*(r^*-1))+(1-\delta^*\alpha^*)(\frac{1}{1+\delta^*\alpha^*(r^*-1)}-1)$$
$$+\frac{(1-\delta^*\alpha^*)^2}{2}(\frac{1}{[1+\delta^*\alpha^*(r^*-1)]^2}-1)] \;/\; [lnr_o^*-\ln(1+\delta^*\alpha^*(r_o^*-1)) \qquad (1)$$
$$+(1-\delta^*\alpha^*)(\frac{1}{1+\delta^*\alpha^*(r_o^*-1)}-1)+\frac{(1-\delta^*\alpha^*)^2}{2}(\frac{1}{[1+\delta^*\alpha^*(r_o^*-1)]^2}-1)]$$

Once the geometry (α^*) of the seal is specified, the pressure distribution depends only on δ^*, the dimensionless coning. As δ^* increases, the pressure distribution becomes more convex, resulting in a larger opening force. For a given closing force, there is a unique value of δ^* (δ/h_i) that produces an equal opening force. Once this value is found, it is then only necessary to compute the dimensional coning δ, to find the steady state film thickness h_i.

To compute δ, one must determine the deformations of the seal components due to pressure loading, thermal stresses, and voltage applied to the piezoelectric element. This is done using the finite element code ANSYS. As input to the finite element program, the viscous heat generation rate in the fluid film is expressed as,

$$Q=\int\frac{\mu\omega^2r^2}{h}dV \qquad (2)$$

where a linear radial profile is assumed for h. Once the viscous heat generation rate is computed, it is apportioned between the seal faces based on their relative thermal resistances.

Since the thermal deformations depend on the film thickness (through Q, eq. (2)), and since the film thickness depends on the thermal deformations, an iterative computational procedure is necessary. Figure 4 contains a flowchart of the computational scheme. Initially, the film

thickness is computed assuming the viscous heat generation rate is zero. The heat generation rate is then computed based on this initial film thickness, and the film thickness is recomputed. This process is repeated until the new values of film thickness and seal component temperatures are equal to the old values, within specified tolerances.

Once the film thickness is known, the leakage rate can be obtained by integrating the pressure gradient at the seal ID, across the thickness of the film. Assuming a linear radial profile for h, an analytical expression for the leakage rate is obtained,

$$m=[-\pi(P_o^2-P_i^2)(h_o-\beta r_o)^3] \;/\; 12\mu RT\;[\ln(\frac{r_o}{r_i})-\ln(\frac{h_o}{h_i}) +(h_o-\beta r_o)(\frac{1}{h_o}-\frac{1}{h_i})+\frac{(h_o-\beta r_o)^2}{2}(\frac{1}{h_o^2}-\frac{1}{h_i^2})] \quad (3)$$

A series of voltage loads is supplied for each computational run. The results obtained from each run include the film thickness, leakage rate, coning, temperature distributions of the seal components, and the pressure profile within the fluid film.

Two additional parameters of interest are the stiffness and controllability of the seal. The stiffness is important to the stability of the seal, and is defined by,

$$k=-\frac{dF_{open}}{dh_i} \quad (4)$$

The stiffness must be positive for stable seal operation, and must be large enough to prevent large fluctuations in the film thickness due to small changes in the closing force. It can be expressed in terms of δ, and δ^* as,

$$k = \frac{dF_{open}}{d\delta^*} \frac{\delta^{*2}}{\delta} \tag{5}$$

For fixed values of $dF_{open}/d\delta^*$ and δ, the seal stiffness increases as δ^* increases.

The controllability of the seal is a measure of the sensitivity of the film thickness to changes in voltage, and is defined as,

$$\frac{dh_i}{dv} = \frac{dh_i}{d\delta} \frac{d\delta}{dv} \tag{6}$$

A large controllability is desirable, to minimize required voltage levels. It can be expressed in terms of δ^* as,

$$\frac{dh_i}{dv} = \frac{1}{\delta^*} \frac{d\delta}{dv} \tag{7}$$

Equation (7) indicates that the controllability of the seal varies directly with $d\delta/dv$, and inversely with δ^*.

As described above, δ^* strongly affects both the stiffness and controllability of the seal. Since

δ^* is determined by the closing force, the latter plays a major role in determining the stability and controllability of the seal.

Figure 5 contains a plot of the seal stiffness versus the closing force for two values of δ, 1 μm and 2 μm. Also presented is a plot of $1/\delta^*$, to which the controllability is proportional. It is seen that maximization of the stiffness and controllability imposes conflicting requirements on the choice of the closing force; maximization of the stiffness requires that the closing force be maximized, while maximization of the controllability requires that the closing force be minimized. Based on Fig. 5, a closing force of 595 N has been chosen, representing a compromise between stability and controllability.

Figures 6 and 7 present typical predicted performance curves for a sealed pressure of 1.48×10^6 Pa (200 psig) and a rotational speed of 3665 rad/sec (35,000 rpm). The initial coning (at 0 volts) has been set at 1.2 μm based on experimental observations (see section on Steady State Results). These performance curves indicate that sufficiently large changes in film thickness can be obtained using the available range of applied voltage.

TEST APPARATUS

The electronically controlled seal is schematically illustrated in Fig. 3. Figure 8 contains a photograph of the principal parts. The housing is constructed of aluminium, while the shaft is

O1 tool steel (19.1 mm maximum diameter). High speed sealed ball bearings (not shown) are used to support the shaft. The floating face holders are boron nitride, which is an electrical insulator but a thermal conductor. The configuration of the face holders was chosen to prevent electrical arcing. Six coil springs load each face holder. The floating faces are resin impregnated carbon graphite, while the nonfloating rotating face is tungsten carbide. A thermocouple is embedded in each carbon face, and the latter is bonded to a PZT-5H piezoelectric crystal (poled in the radial direction) with conducting epoxy. The back side of the crystal is covered by copper foil, which serves as an electrode. Leads attached to the electrode and the carbon-piezoelectric crystal interface allow a voltage to be imposed across the crystal, normal to the poling axis (the carbon side is grounded).

The overall test setup is shown in the schematic of Fig. 9 and the photographs of Figs. 10 and 11. Helium is supplied from a cylinder, and its flow rate (leakage rate) measured by a rotameter. The shaft is driven by a one horsepower variable speed motor through a belt drive. Shaft speed is measured with a tachometer. Cavity pressure is measured with a Bourdon gage, and temperatures (face and cavity) with thermocouples. A DC power supply provides the voltage for the piezoelectric crystal.

STEADY STATE RESULTS

As described above, the intent of the controllable seal design is to allow one to change the thickness of the lubricating film by changing the voltage applied to the piezoelectric element.

The resulting change in film thickness will be accompanied by a change in leakage rate. Figure 12 contains results of a steady state test performed with a sealed pressure of 1.48×10^6 Pa (200 psig) and a rotational speed of 3665 rad/sec (35,000 rpm). Initially, 2000 volts are applied to the piezoelectric element and the leakage rate is measured. The voltage is then reduced in 500 volt steps until a 0-voltage level is reached, after which the voltage is increased in 500 volt steps until a level of 2000 volts is reached. Following each step change, the voltage is held constant for three to five minutes.

The plots of applied voltage and leakage rate (of both seals) versus time, contained in Fig. 12, show that with each reduction in voltage there is a corresponding reduction in leakage rate, and with each increase in voltage there is a corresponding increase in leakage rate. The incremental change in leakage rate decreases with decreasing voltage. Over the decreasing voltage portion of the curves, going from 2000 volts to 0 volts, the leakage rate is decreased from approximately 100 mg/sec to 10 mg/sec. Over the increasing voltage portion of the curve, going from 0 volts to 2000 volts, the leakage rate is increased from approximately 10 mg/sec to 125 mg/sec. These results have also been plotted in Fig. 6, for comparison with the analytical predictions. It is seen that the agreement between the test and analysis results is quite good, considering that the value of the initial coning (at 0 volts) used in the analysis, 1.2 μm, has been chosen on the basis of static measurements of coning (using an optical flat).

Comparison of the decreasing voltage and increasing voltage portions of the curves in Fig. 12 reveals the existence of hysteresis in the seal response. This can be seen both in the total change

in leakage rate (resulting from a 2000 volt change) and the incremental changes. It is believed that this hysteresis is due to hysteresis in the piezoelectric element and hysteresis in the floating seal face component. The latter arises from the sliding of the component relative to the housing. The presence of hysteresis suggests the use of an adaptive control system with this seal. (Such an adaptive control system was used with earlier controllable seals (1, 3).)

Figure 13 contains the temperature histories of the two seal faces and the cavity during the test of Fig. 12. It is seen that all temperatures increase in concert during the portion of the test with decreasing voltage and leakage, and generally decrease in concert during the portion with increasing voltage and leakage. This is expected, since the lower the voltage, the thinner the film and the higher the heat generation rate between the faces. However there is a lag of approximately four minutes between the point of maximum temperature and the point of minimum leakage rate, due to the thermal inertia of the system.

It had been expected that the face temperature, relative to the cavity temperature, would be a good indicator of the conditions in the film, and could be used as the input to a control system that generates a commanded voltage to the piezoelectric element. Figure 14 contains a plot of that relative face temperature for the test described above. Although there is some scatter in the results, it is seen that the lower the leakage rate (and the thinner the film), the higher the relative face temperature. However, the practicality of using the relative face temperature as input to a control system cannot be ascertained until transient tests are performed. An alternative input would be the output from a leakage rate monitor.

The effect of rotational speed can be seen by comparing Fig. 12 with Figs. 15 and 16, which contain the results of similar tests performed at 2723 rad/sec (26,000 rpm) and 3246 rad/sec (31,000 rpm). Although there are some variations, the seal behavior is qualitatively similar at all three speeds. It appears, however, that the hysteresis increases with decreasing speed.

Figures 17 and 18 contain the results of tests with sealed pressures of 7.91×10^5 Pa (100 psig) and 1.14×10^6 Pa (150 psig), and a rotational speed of 3246 rad/sec. Comparison with Fig. 16, indicates that the same qualitative behavior occurs regardless of sealed pressure. However, as would be expected, the lower the sealed pressure, the lower the leakage rate. This is due to both the reduced pressure drop across the seal, and the reduced film thickness at lower sealed pressures. It should also be noted that the lower the sealed pressure, the more pronounced the hysteresis and the lower the controllability at low voltages.

CONCLUSIONS

The results of this study, so far, indicate that an electronically controlled mechanical seal for aerospace applications is feasible. Such a seal, meeting the required size constraints, has been built, and has generally performed as expected under steady state conditions. The steady state tests have shown that the leakage rate (and film thickness) can be adjusted over a substantial range, utilizing the available range of voltage. The next step in this study is a series of transient tests.

REFERENCES

1. Salant, R.F., Miller, A.L., Kay, P.L., Kozlowski, J., Key, W.E. and Algrain, M.C., "Development of an Electronically Controlled Mechanical Seal," in *Proc. 11th Intl. Conf. Fluid Sealing*, Nau, B.S., ed., BHRA, Cranfield, UK (1987), pp. 576-595.

2. Heilala A.J. and Kangasniemi A., "Adjustment & Control of a Mechanical Seal Against Dry Running & Severe Wear," in *Proc. 11th Intl. Conf. Fluid Sealing*, Nau, B.S., ed., BHRA, Cranfield, UK (1987), pp. 548-575.

3. Salant R.F., Giles O. and Key W.E., "Design of Controllable Mechanical Seals," in *Tribological Design of Machine Elements*, Dowson, D., ed., Elsevier, Amsterdam, The Netherlands (1989), pp. 47-55.

4. Etsion I., Palmor Z. and Harari N., "Feasibility Study of a Controlled Mechanical Seal," STLE/ASME 1990 Tribology Conference Preprint **90-TC-2D-1**.

5. Wolff, P.J., "Development of an Actively Controlled Mechanical Seal," Georgia Institute of Technology, Atlanta, Ga., Master's Thesis (1991).

LIST OF FIGURES

Fig. 1

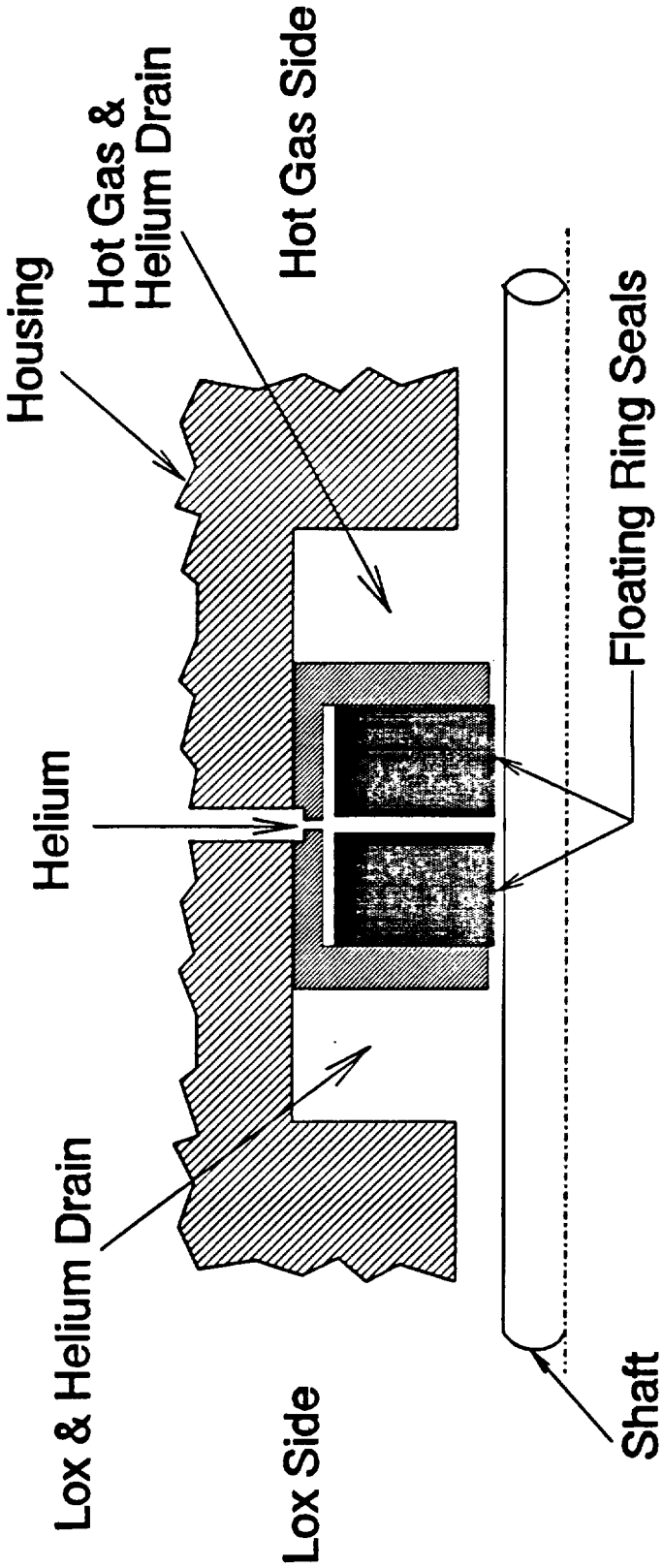
Housing
Hot Gas &
Helium Drain
Hot Gas Side
Helium
Floating Ring Seals
Lox & Helium Drain
Lox Side
Shaft

Fig. 2

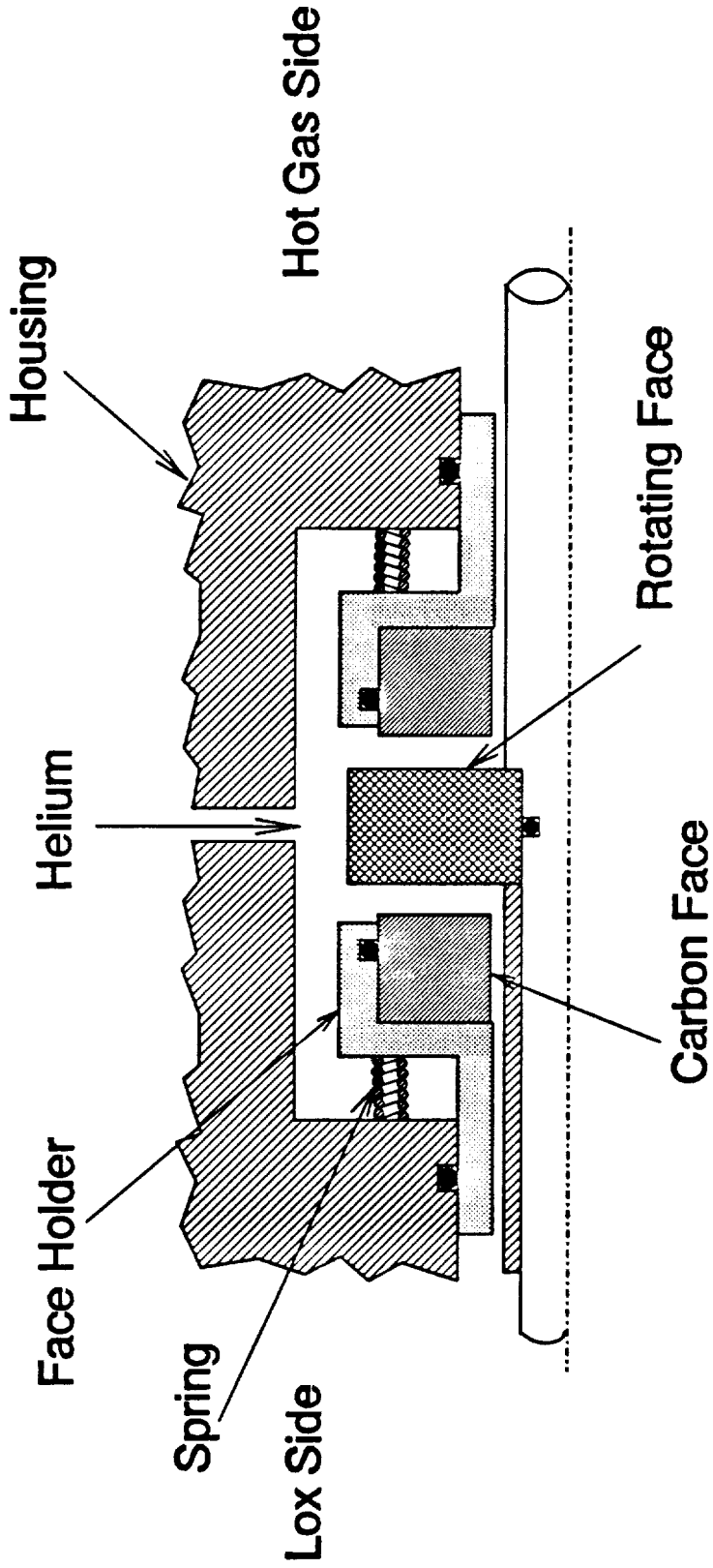
Housing
Hot Gas Side
Helium
Rotating Face
Carbon Face
Face Holder
Spring
Lox Side

Fig. 3

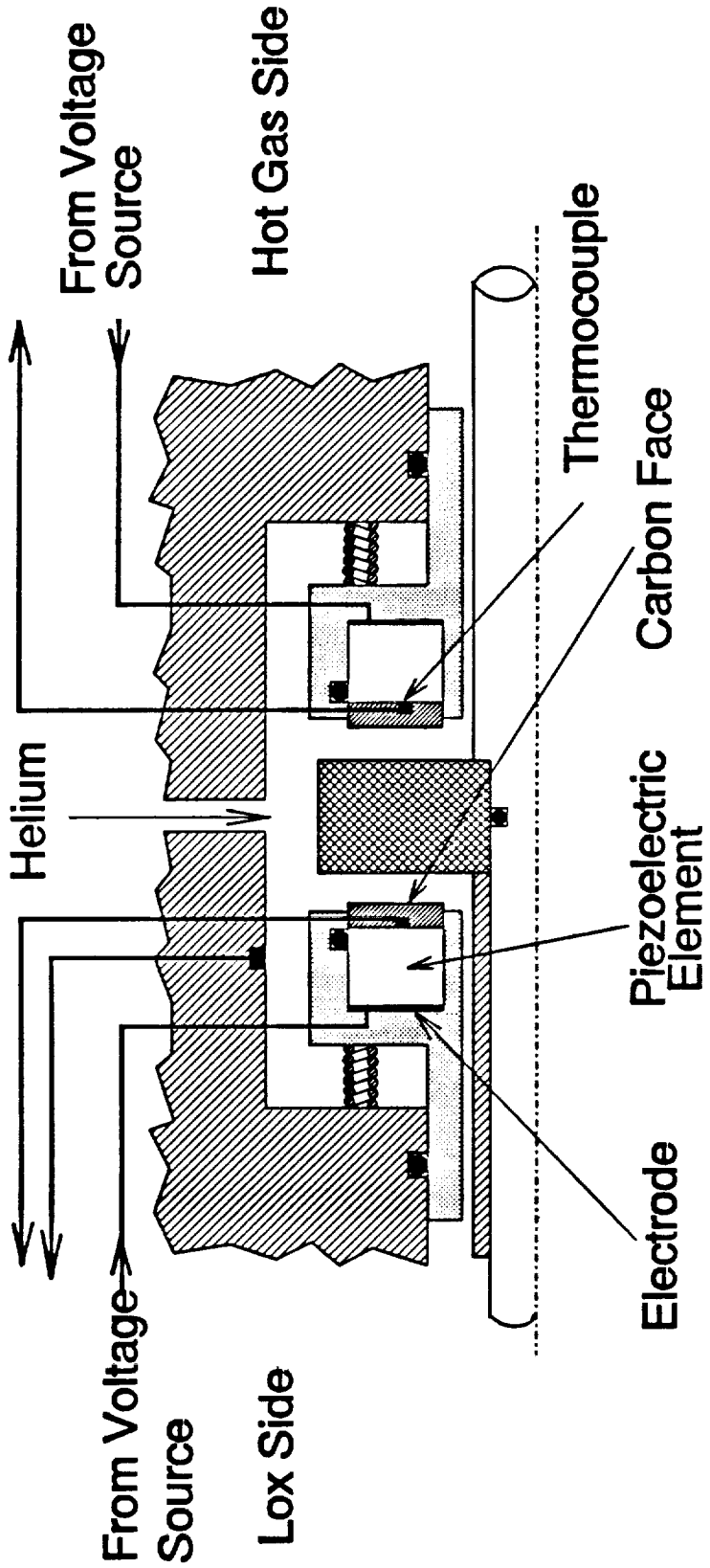
From Voltage Source
Hot Gas Side
Thermocouple
Carbon Face
Helium
Piezoelectric Element
Electrode
From Voltage Source
Lox Side

Fig. 4

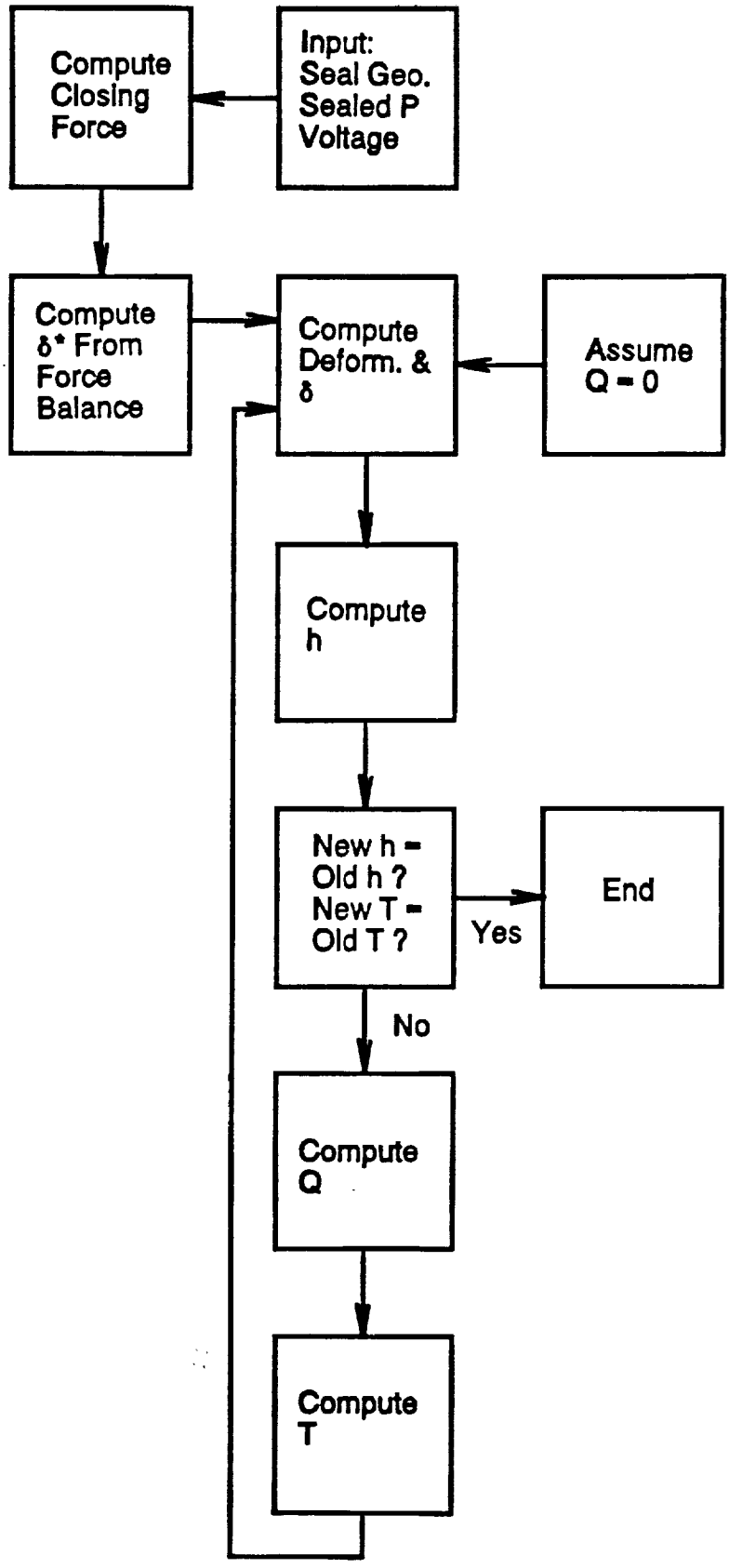
Compute Closing Force
Input: Seal Geo. Sealed P Voltage
Compute δ* From Force Balance
Compute Deform. & δ
Assume Q = 0
Compute h
New h = Old h ? New T = Old T ?
Yes
End
No
Compute Q
Compute T

Fig.5

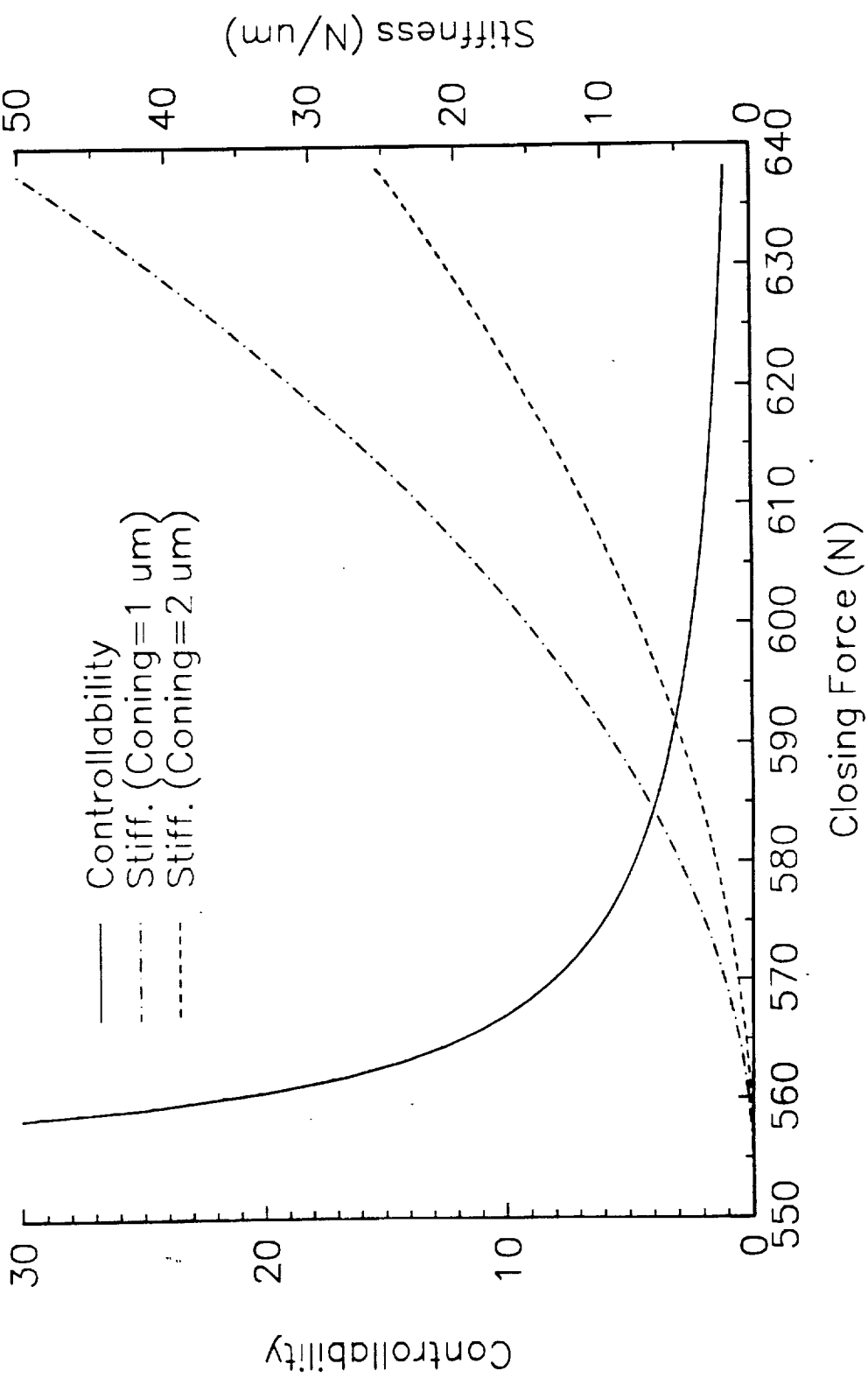
Controllability
Stiff. (Coning=1 um)
Stiff. (Coning=2 um)
Controllability
Stiffness (N/um)
Closing Force (N)
0
10
20
30
40
50
550
560
570
580
590
600
610
620
630
640

Fig. 6

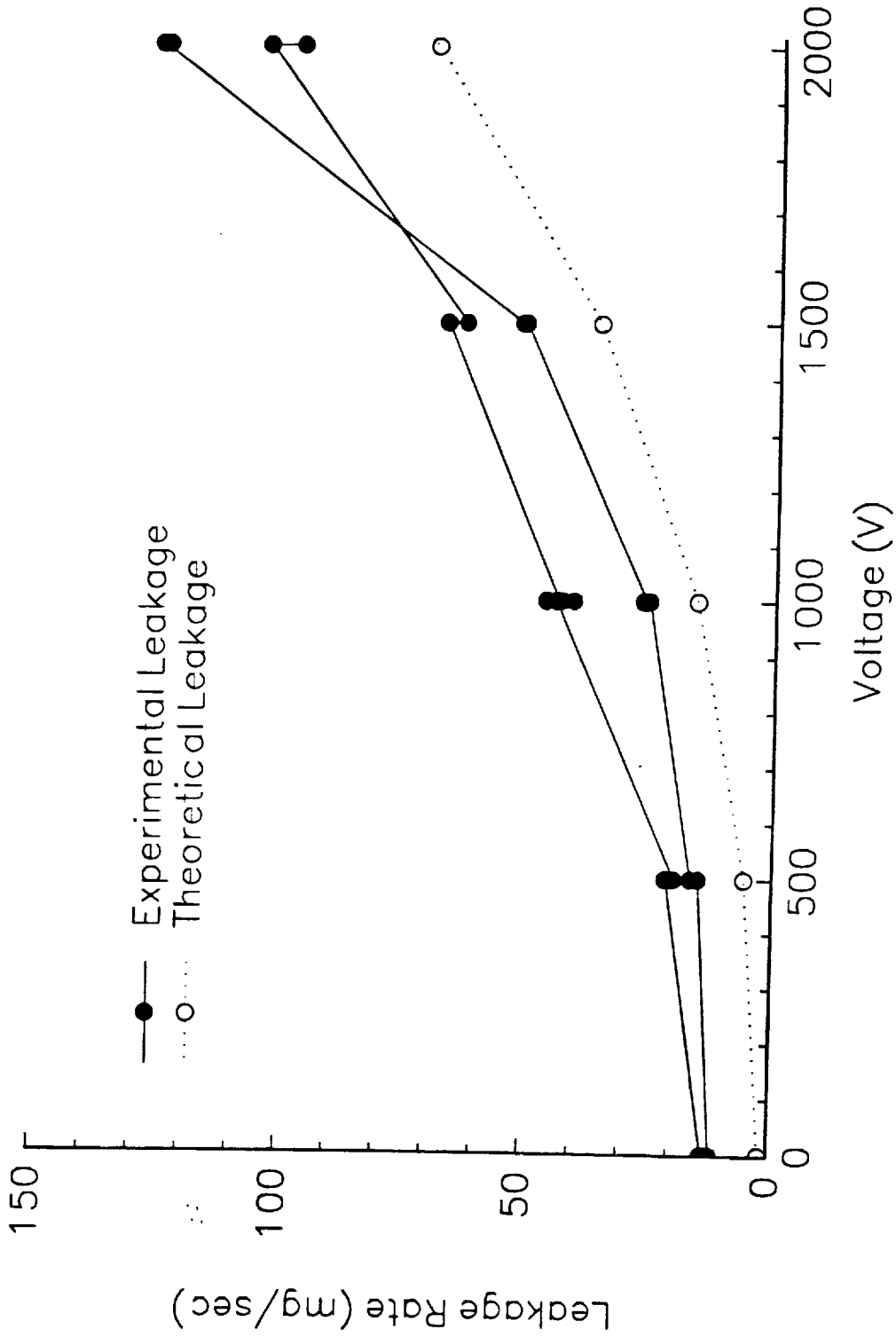
Leakage Rate (mg/sec)
150
100
50
0
0
500
1000
1500
2000
Voltage (V)
Experimental Leakage
Theoretical Leakage

Figure 7

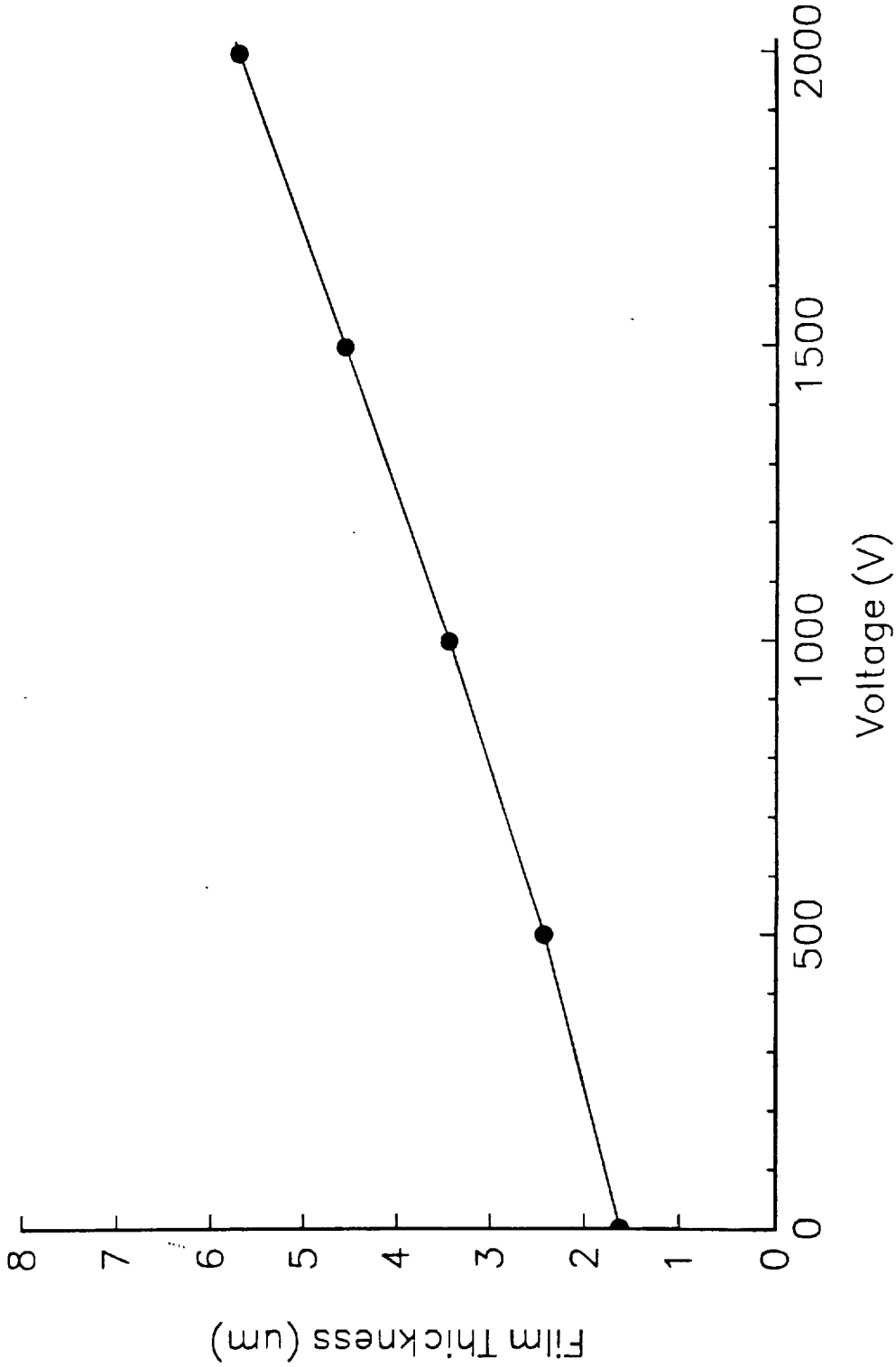

Fig. 8

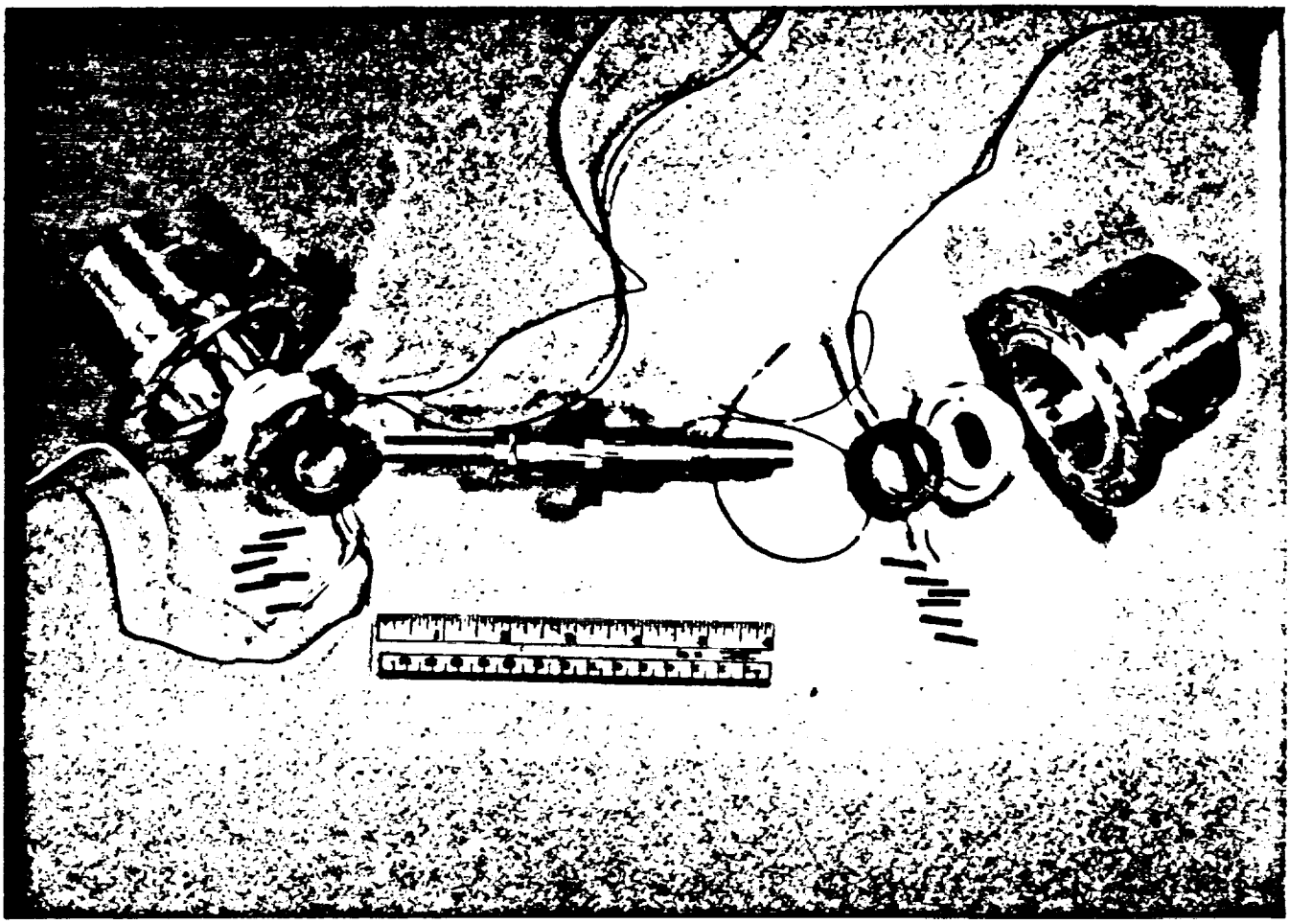

Fig. 9

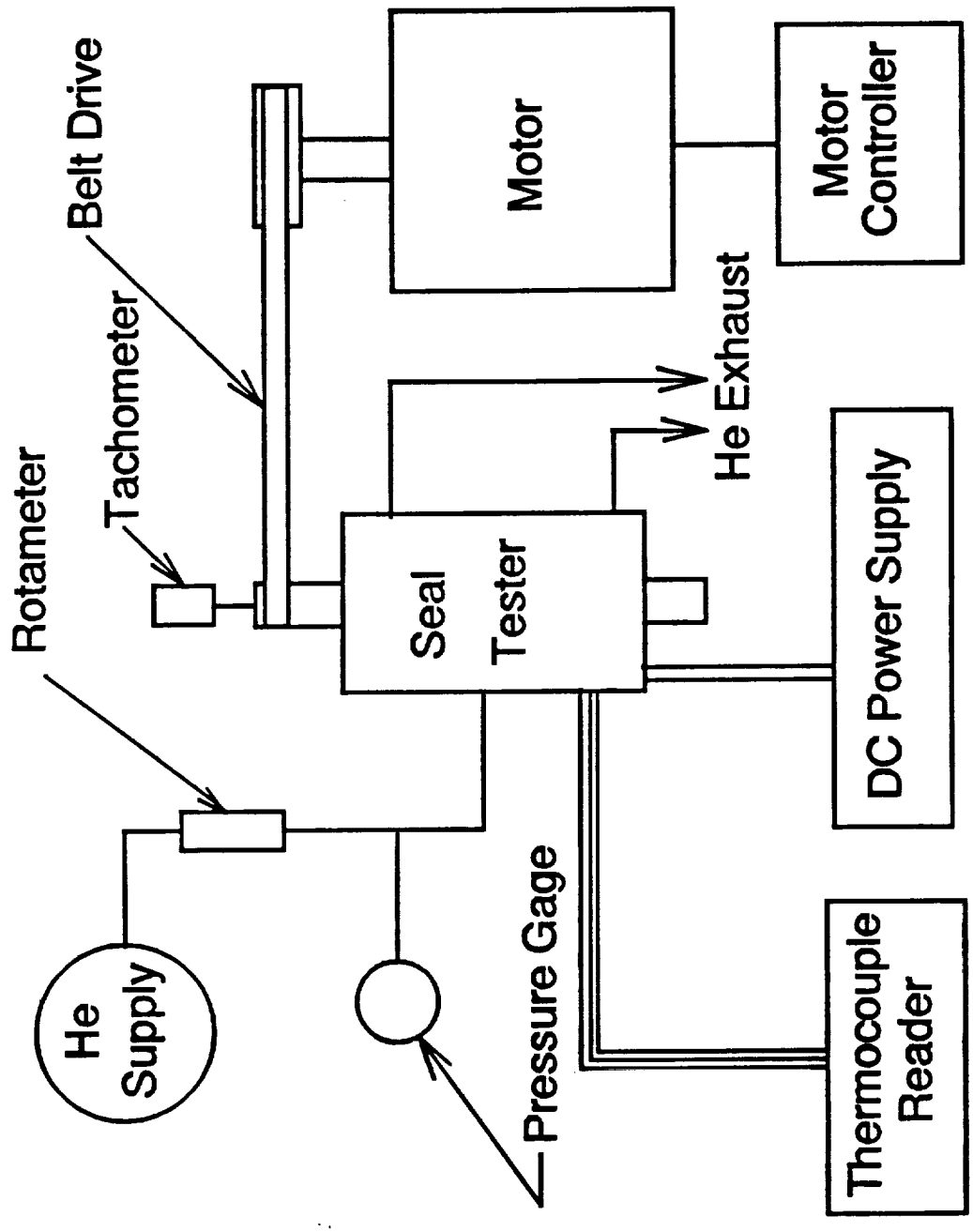
Belt Drive
Tachometer
Rotameter
Motor
Motor Controller
He Exhaust
Seal Tester
DC Power Supply
He Supply
Pressure Gage
Thermocouple Reader

Fig. 10

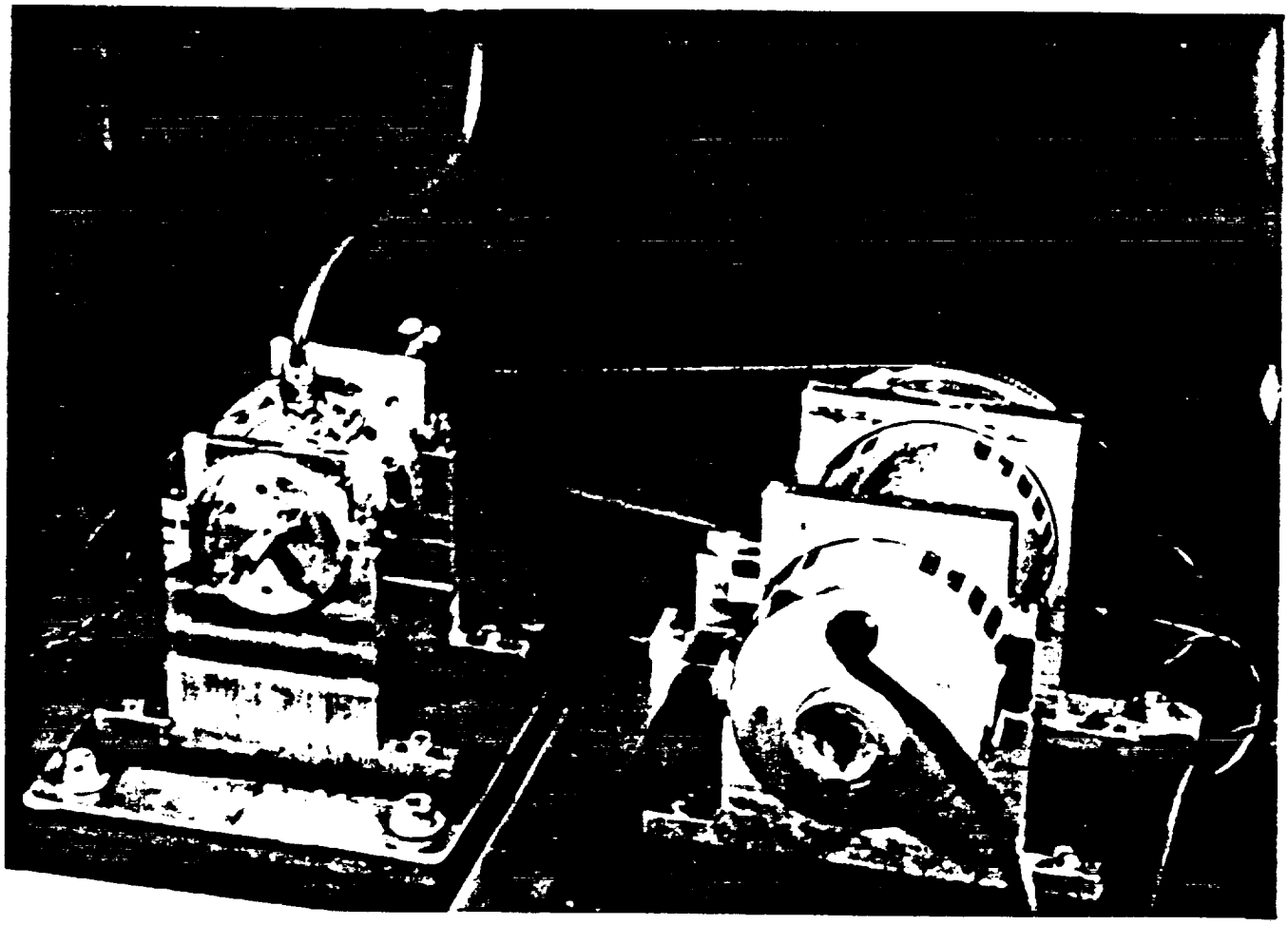

Fig. 11

Fig. 12

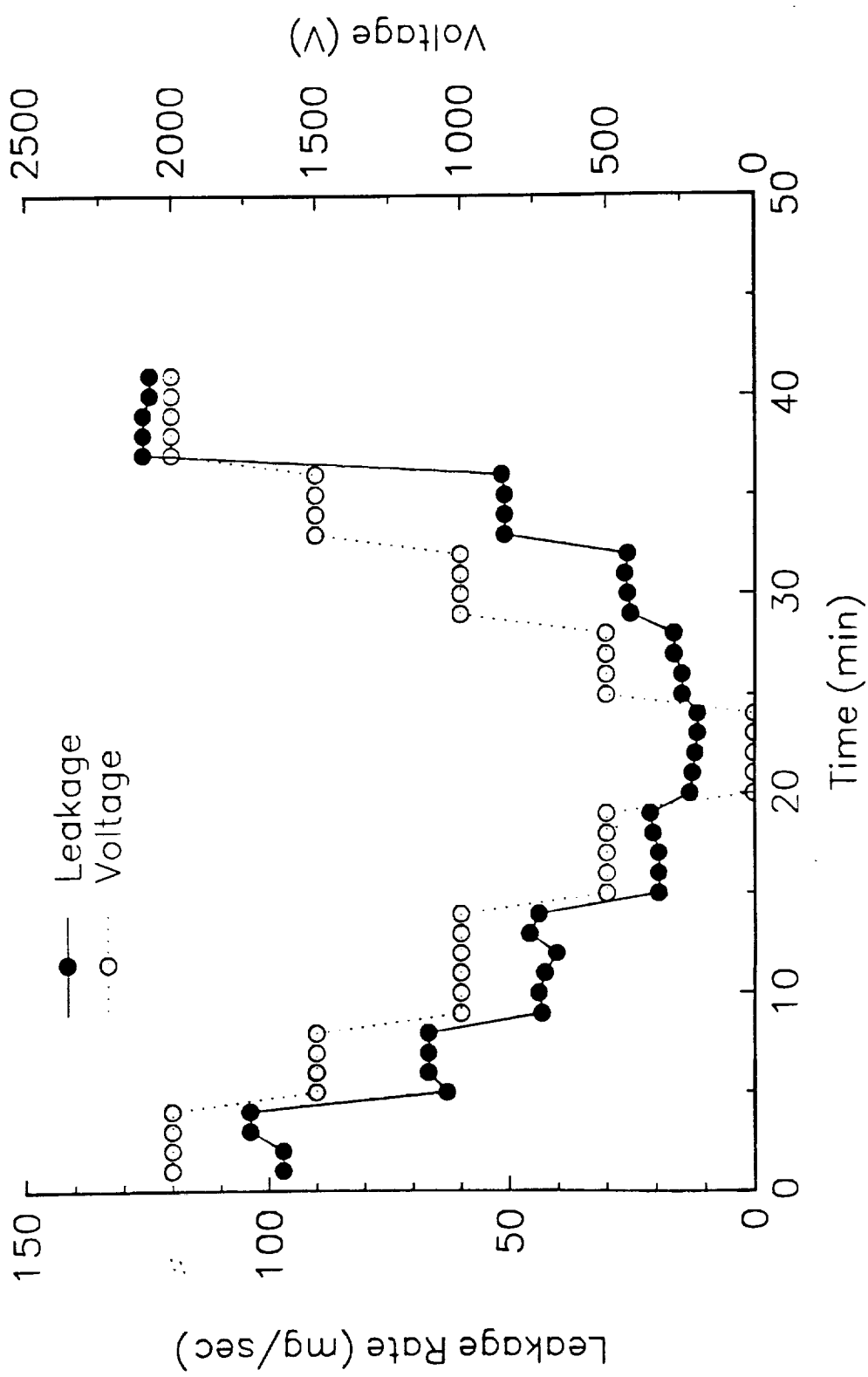
Leakage Rate (mg/sec)
Voltage (V)
Time (min)
Leakage
Voltage
150
100
50
0
2500
2000
1500
1000
500
0
10
20
30
40
50

Fig. 13

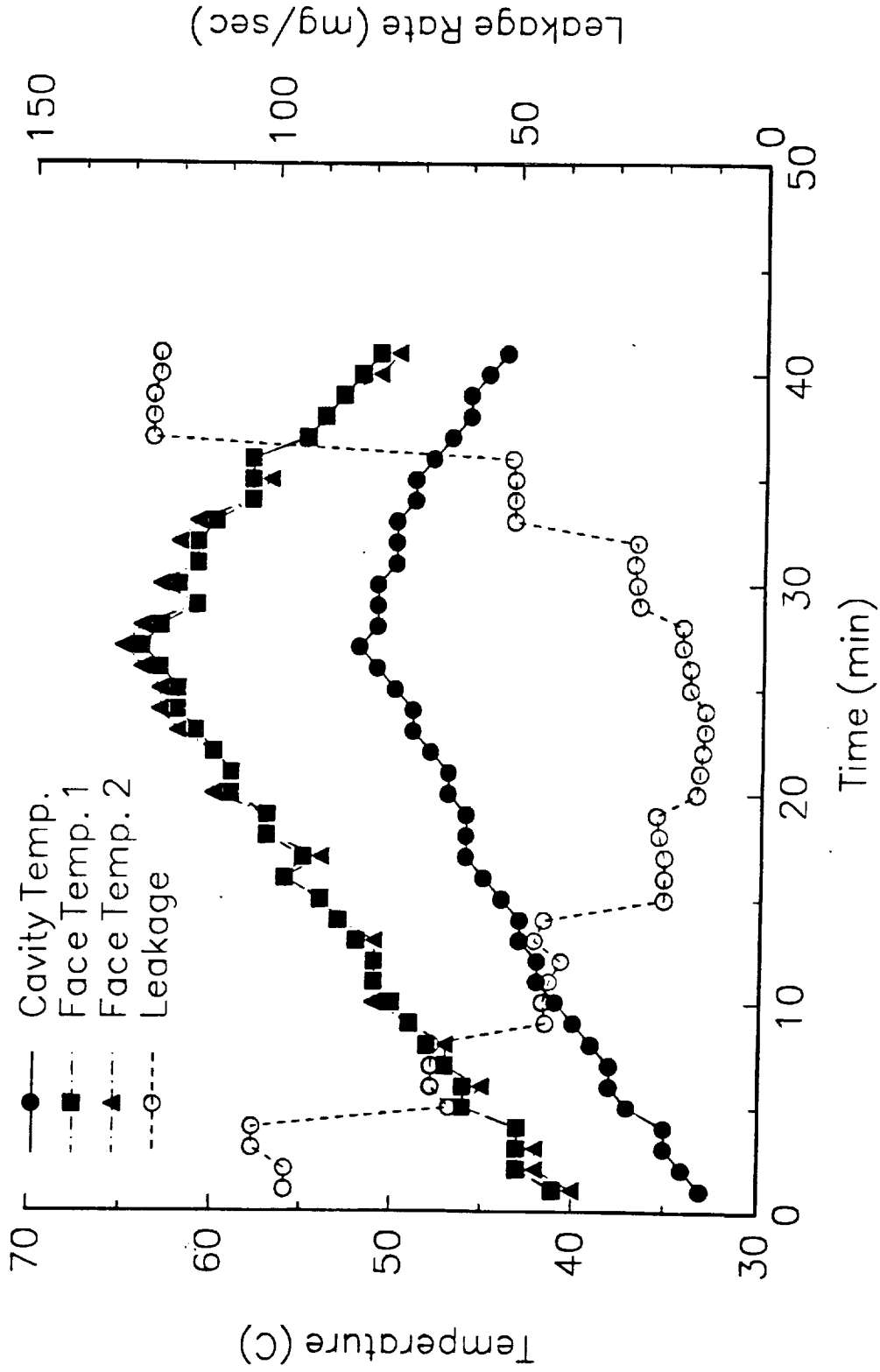
Leakage Rate (mg/sec)
150
100
50
0
50
40
30
20
10
0
Time (min)
Temperature (C)
70
60
50
40
30
Cavity Temp.
Face Temp. 1
Face Temp. 2
Leakage

Fig. 14

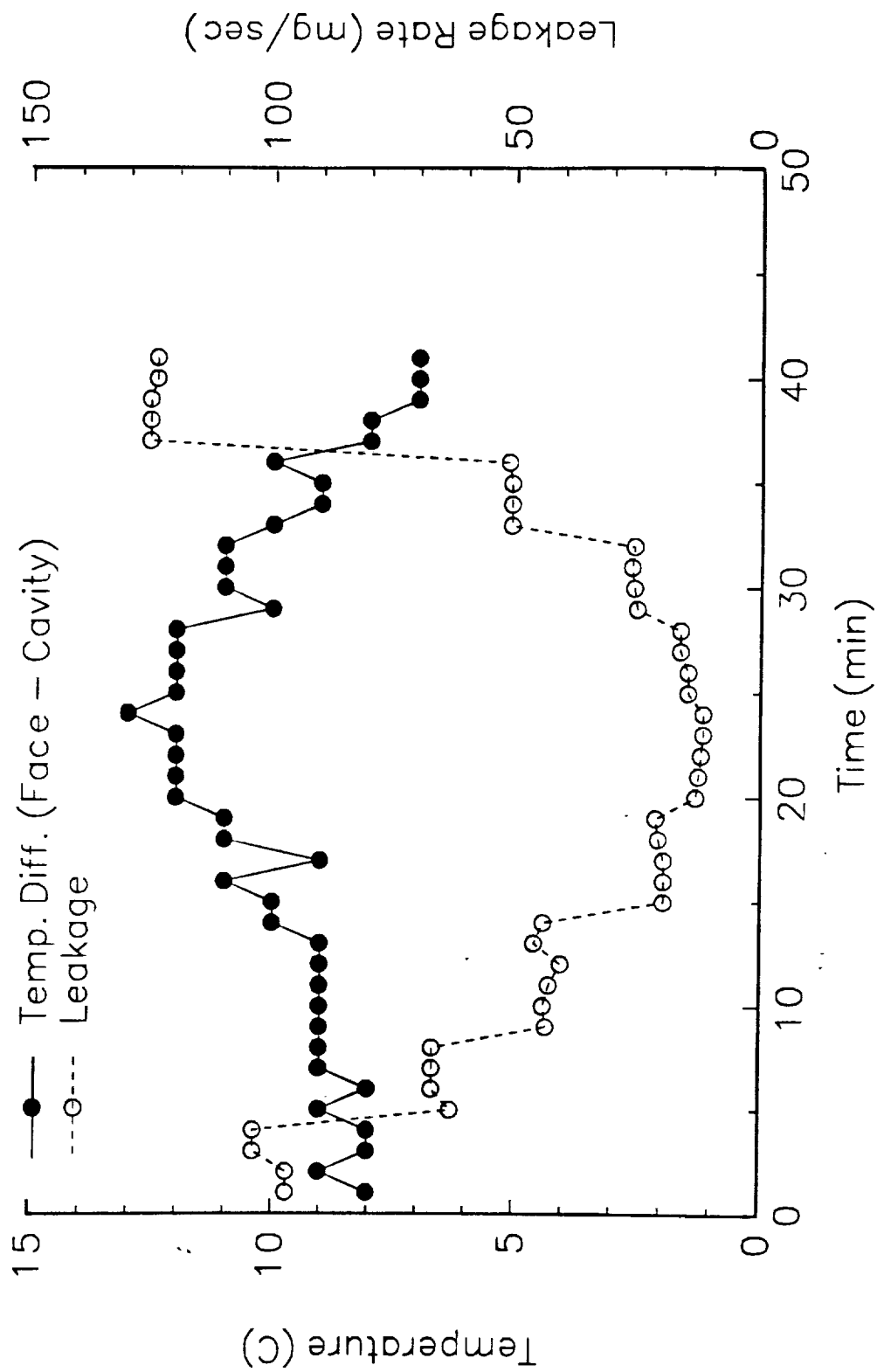
Leakage Rate (mg/sec)
150
100
50
0
50
40
30
20
10
0
Time (min)
Temperature (C)
15
10
5
0
Temp. Diff. (Face – Cavity)
Leakage

Fig.15

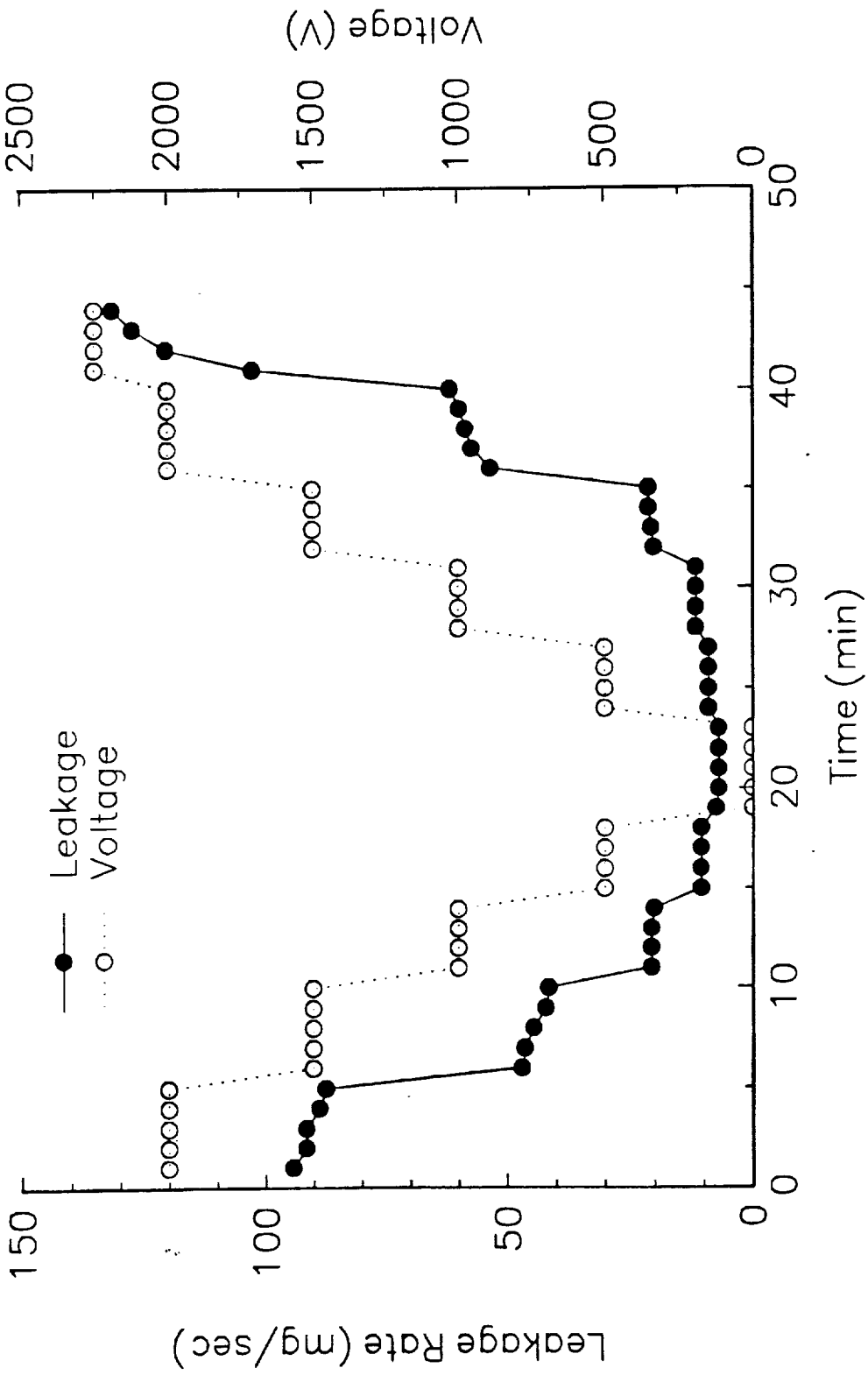
Leakage Rate (mg/sec)
Voltage (V)
Time (min)
Leakage
Voltage
150
100
50
0
2500
2000
1500
1000
500
0
0
10
20
30
40
50

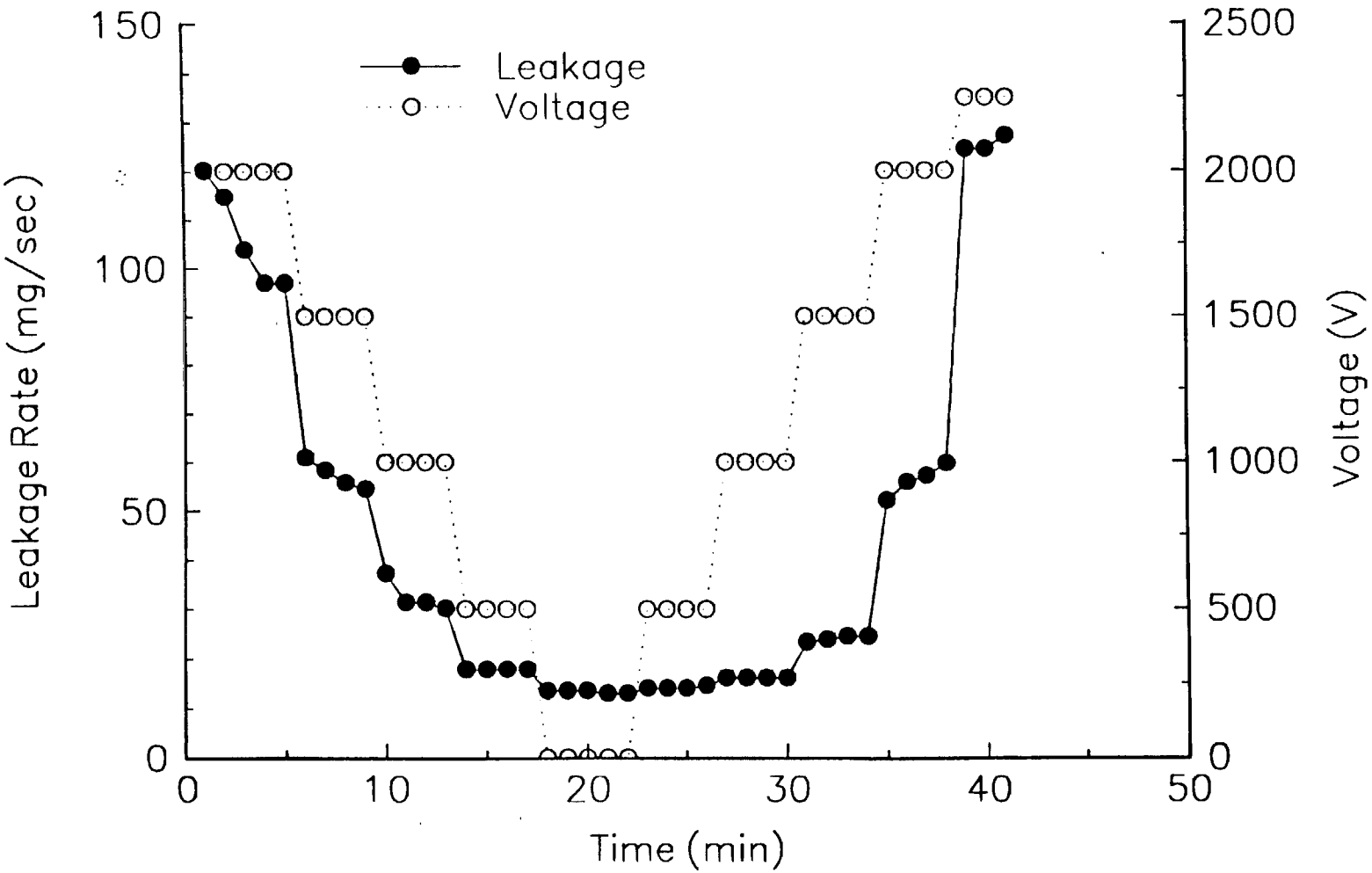
Leakage
Voltage
Leakage Rate (mg/sec)
Voltage (V)
Time (min)
150
100
50
0
2500
2000
1500
1000
500
0
0
10
20
30
40
50

Fig. 16

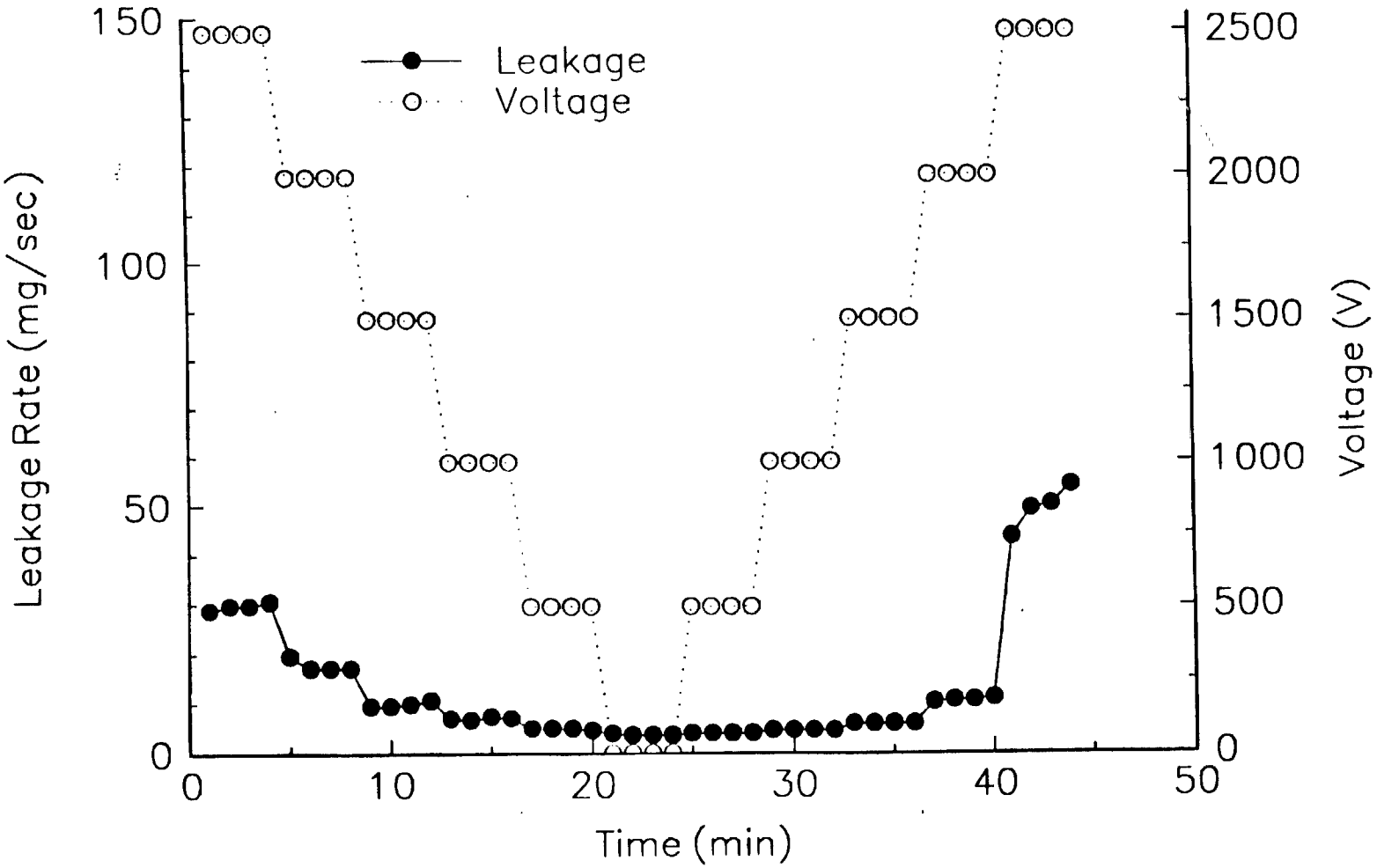
Leakage
Voltage
Leakage Rate (mg/sec)
Voltage (V)
Time (min)
150
100
50
0
2500
2000
1500
1000
500
0
0
10
20
30
40
50

Fig.17

Fig. 18

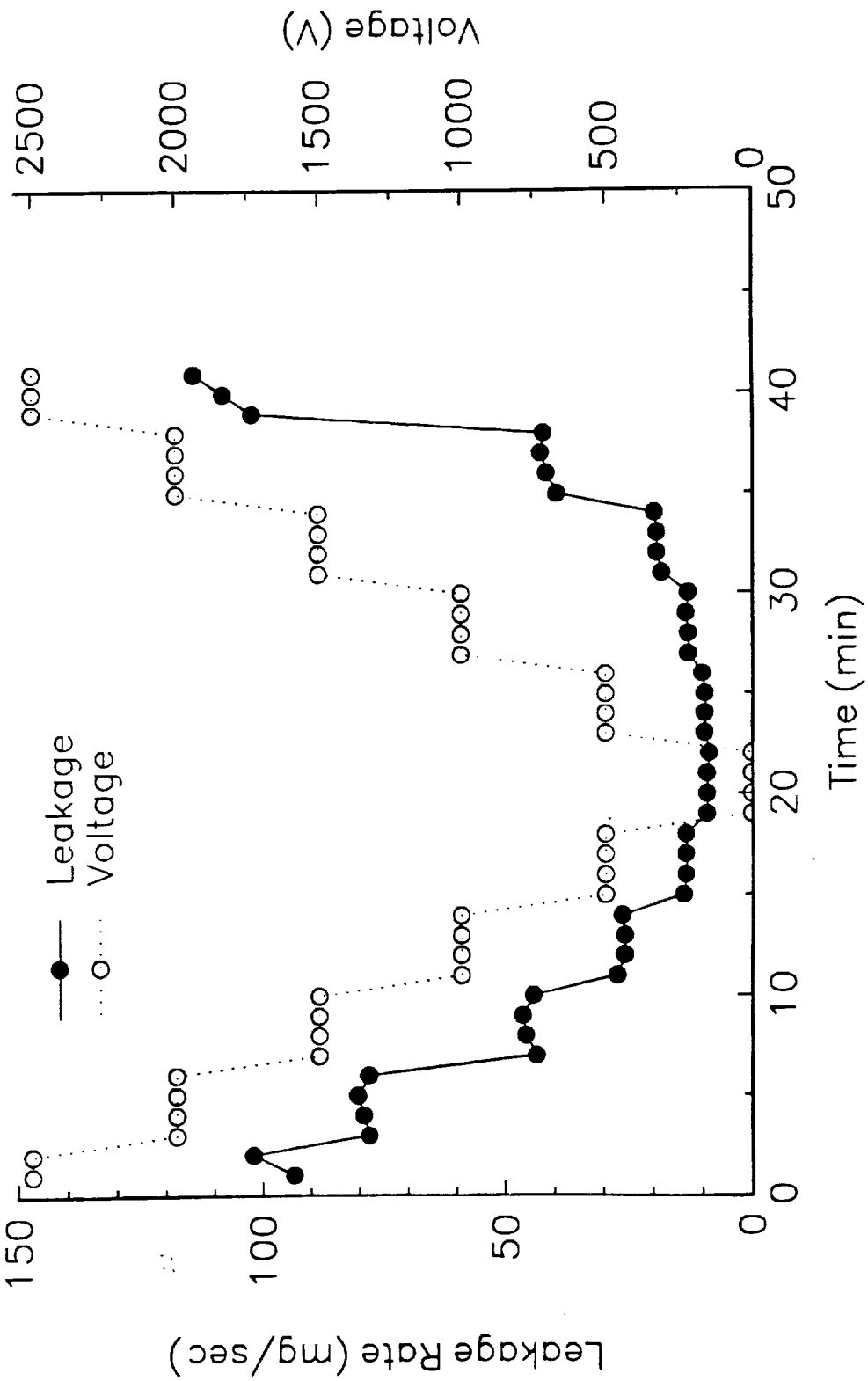
Leakage Rate (mg/sec)
150
100
50
0
Voltage (V)
2500
2000
1500
1000
500
0
0
10
20
30
40
50
Time (min)
Leakage
Voltage